Chiang Mai J. Sci. 2016; 43(6) : 1324-1334
http://epg.science.cmu.ac.th/ejournal/
Contributed Paper

Structural Analysis of Part of the Nigerian South-western Basement Complex using Aeromagnetic Data

John S. Kayode*, Mohd Nawawi and Khiruddin Abdullah
Geophysics Unit, Universiti Sains Malaysia, School of Physics, 11800 USM, Penang, Malaysia.
* Author for correspondence; e-mail: jskayode@gmail.com

Received: 21 February 2016
Accepted: 8 July 2016

ABSTRACT

Valuable and precious subsurface minerals have been continuously mined illegally in the region of Omu-Aran area in parts of the Nigerian South-western Precambrian Basement Complex. An aeromagnetic data obtained from the Nigerian Geological Survey Agency was analysed to delineate various subsurface geological structures in this area. The subsurface characteristics enrichment of the data was carried out using Fast Fourier Transforms, and the Euler Deconvolution methods that helped in the establishment of the different subsurface magnetic anomalies basement structures emplaced in this part of the Nigerian South-western Precambrian Basement Complex. The study aimed at mapping the main rock types found in the undifferentiated schist that includes some gneiss, schist, quartzite and quartz schist and granite-gneiss in the basement rocks of the area. It also includes delineating, as well as estimating the depths to, the magnetic source of the Ore bodies. Regional- residual separation was applied to the total aeromagnetic data to produce a total magnetic intensity map with the application of Oasis Montaj (2014 software version). Depths to the shallow magnetic anomalies source rock bodies were estimated together with various structural indices that varied between about 0.5SI and 3.0SI at the greatest depth to the shallow anomaly of about 1100m, with the aim of determining the greatest depths approximation for all the subsurface geological structural features in the area.

Keywords: aeromagnetic data, magnetic source anomalydepths, Precambrian basement complex, Nigeria

1. INTRODUCTION

Mapping of geologic structures such as geological boundaries, fractures, and faults are successfully accomplished using the applications of potential field geophysical prospecting methods. These geophysical methods have been useful in a diversity of ways to provide helpful information about the subsurface basement geological structures that may reflect the greater potential for the occurrence of mineralized rocks in a particular area. Magnetic methods of geophysical prospecting have been successful because

of the relatively high magnetic susceptibility contrast between basement rocks units and these mineralized units [1, 2]. Potential-field geophysical prospecting methods have been shown to provide information within which subsurface structural geological features emerge. These techniques do not deal only with the applications of the methods to explore valuable and precious subsurface materials, but also find significance in the Oil and Gas Prospecting, [3]. It has been fully established in the geoscientific world, that integrating geophysical studies is a key to understanding the subsurface features, more importantly when the applications of magnetic and gravity are coupled with other methods. These geophysical methods have been well developed for nearly a century, but significant achievements through the introduction of computer software and improved digital mechanisms for data acquisition increases the scope of applications and reduce costs significantly.

The total intensity aeromagnetic map of Nigeria Basement Complex recently published by the Nigerian Geological Survey Agency provides an opportunity for researchers to access the data. The data was acquired at average intervals of 0.1s, which covered the entire country through, Fugro Airborne Survey Services and Patterson Grant and Watson (PGW), Canada, from 2003 to 2009, [4]. The aeromagnetic coverage over most areas of the country was acquired through a sequence of Northwest-Southeast flight lines that are transverse to the major local geological strike. The data was collected at an average line spacing of 0.5 km, with 2 km tie-line spacing in the Northeast-Southwest directions and 80m low flights height, [4].

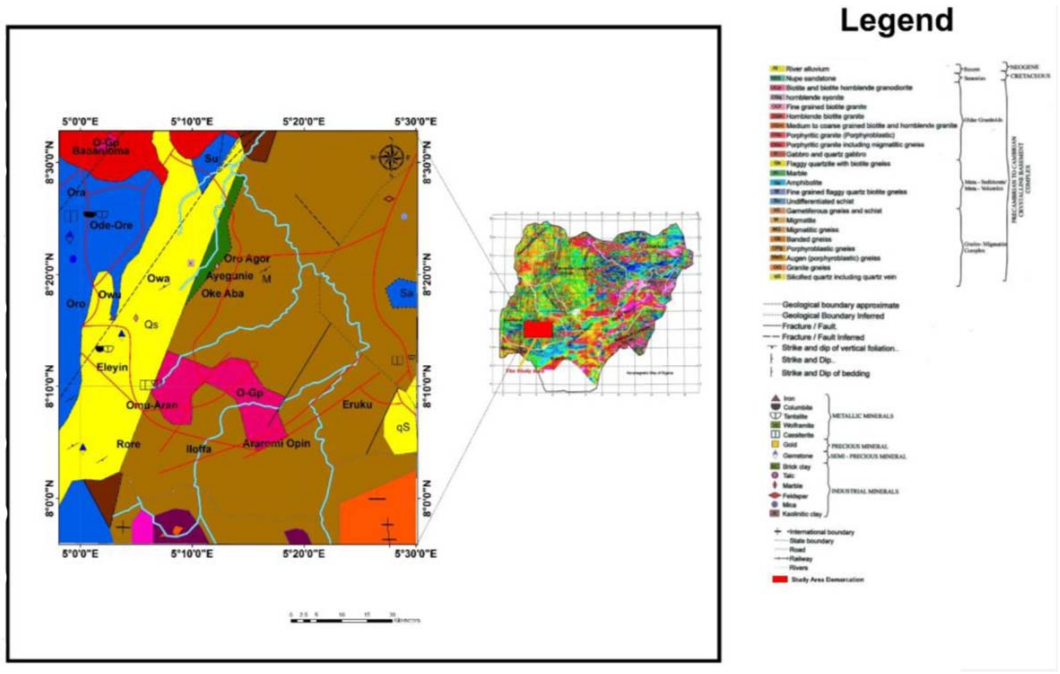

Figure 1. The Geological map showing the survey area as adapted from the Nigerian Geological Survey Agency.

The study area lies within the South-western schist belt and surrounded by Longitudes 4° 59′ 47.26″ E and 5° 29′ 57.95″ E, and Latitudes 7R 59′ 45.6″ N and 8° 30′ 22.21″N, (Figure 1). The South-western part of the Nigerian schist belts are well-developed in the country alongside the Western border of of the study area at Longitudes, 4° E to 8° E and Latitudes, 6° N to 10° N. Insignificant amounts of schist formations were recognised in the eastern area, although occasionally. As shown in Figure 1, the Nigerian schist belts are confined to NNE-trending zones across a width of about 300km, [5, 6, 7, 8]. Gneisses and migmatites that constitute the Dahomeyan units made up some of the region to the West of this geographical area. Likewise to the East of the Nigerian South-western schist belt, spanning a region up to about 700km wide, there is no known existence of schist rocks with the exception of Cameroun where varieties of these types of rocks, thought to be of the Upper Proterozoic age, crop out within the Pan-African granite-migmatite terrain sited in the northern part of the Congo Craton, [8, 9,10].

Variations in the angle of inclination of the Earth's geomagnetic fields between 0° and 35° makes it imperative to apply a Reduced to Pole (RTP) filter to the magnetic data, for improved image of the magnetic anomalies produced. Also, we applied the first vertical derivative filter on the map generated by the application of the RTP filter. These procedures provided an improved knowledge of the shallower geological structures in the area. This study, therefore, presents the interpretations we carried out, arising from the maps generated from the results of the structural indices, the analytical signal of total magnetic intensity map, the reduced to pole map, and derivatives maps.

From the analysis, we implemented in this work, the regional subsurface geology and subsurface structural features of these parts of the Nigerian South-western Precambrian Basement Complex studied was well-delineated, as shown in all the maps produced. In general, the south-western granulite terrain is distinctive from the other structural features in the area through the high magnitude and high-frequency magnetic anomalies recorded. The ridge-like structures controlling the Schist Belt anomalies could be clearly seen trending along the NNE directions.

Many workers have previously reported published work on the Nigerian Precambrian Basement Complex, using a range of approaches, i.e., [8, 9, 11, 12, 13, 14, 15]. All applied magnetic methods in diverse ways to delineate geological structures in some parts of the Nigerian Precambrian Basement Complex. The Ilesha schist belts, nearby to the present study area in the South-western part of the schist belt complex, have been well documented through some of this research in the Nigerian South-western area.

The current study is aimed to map out the magnetic anomalies produced by ore rock bodies, controlled by the Nigerian South-western Basement geological structures that support subsurface precious minerals deposits. Here we also map out the subsurface basement environment that has the potential for precious and valuable solid mineral prospects using the aeromagnetic method of geophysical prospecting.

Ten Brink and others [17] worked in northern part of the present study area, also, Megwara and Udensi [18], worked in Okemesi the next southern part of the Omu-Aran schist belt using LANDSAT TM.

On the whole, the present study area, namely the Omu-Aran schist belt, is yet to have had and significant geological and

geophysical work. Illegal miners have taken advantage of the present geoscientific information gap to undertake their illicit business; that has propelled this study to bring the zone to the attention of researchers in the mining and geosciences fields.

2. MATERIALS AND METHODS

The aeromagnetic data was acquired from the Nigeria Geological Survey Agency, covering the study area, gridded and contoured after the applications of the usual corrections and was processed using the flowchart presented in Figure 2. It is, therefore, mandatory to improve the signal of the data through separation of the shortwave, (local) and the long wave, (residual) components of the total field anomalies data. The former represent shallow magnetic anomalies, (i.e., the near-surface sources) while the later represent the deep-seated magnetic anomalies sources respectively. The task was accomplished via the application of a Low Pass Filter (LPF) for the elimination of higher frequency and noisy signals in order to shape the spectrum that will improve the importance of subsurface basement complex geological features such as, the bedrock topography, faults /fractures and the contacts between two or more rocks,[19].

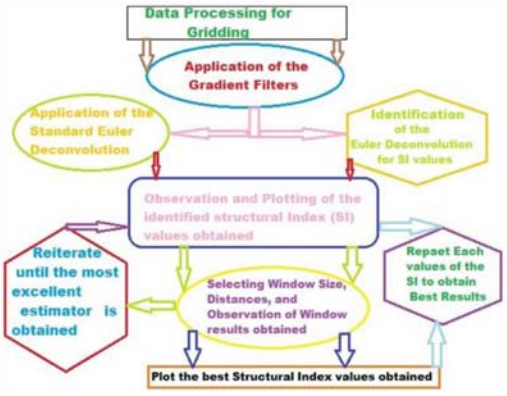

Figure 2. The Workflow for the data processing and interpretations.

The LPF applied to remove all forms of irregularities and disturbances from the input data through the use of convolution filtering. This process permits the passage of low or substantial wave numbers to be passed to the output file. In doing this, attributes that are shorter than the short wavelengths are discontinuous and automatically eliminated from the output data generated with a minimal other effects. Geosoft Inc. applied [20] in the design of this filter as implemented in the Oasis Montaj8.3 version released in 2014, [20, 21, 22]. To put a constraint on the range or band of this filter, a Band pass filter was equally applied also to eliminate the long-wavelength signals completely. The disadvantage of LPF is in its linearity as it handles all the data equally. During the process, a part of the very high amplitude attributes are removed alongside the short wavelength signals and this creates problems in the output data as some parts of the data not predetermined to be eliminated are removed.

When the above problem arises, we are left to adopt a Non-linear filtering technique. This filter is best for the removal of the high amplitudes attributes and slow-moving wavelength noisy signals from the data without removing any part of the data as we experienced in the LPF. Non-Linear Filtering is considered as a "Noise Spike Rejection Filter," (NSRF), [21, 22, 23, 24]. NLFT is also very effective in the removal of one-dimensional geological short-wave features from the data as we have in secondary structures. In the high pass, low pass, and band pass filters, as linear filters, the algorithm altered the data in an attempt to remove some noisy signals, thereby creating problems in the output generated. On the other hand, the non-linear filters use an algorithm that can identify and recognise a data point as

being noisy or true frequency through thorough examinations by the nearest neighbour data points and hence add or otherwise removed if it is noise. Non-linear filters algorithm entrenched its judgments on the amplitudes and width of attributes in the data on the regional environment. In this process, geological features with narrow width and higher magnitudes than that detailed by the filter will be treated as noise and therefore, be removed. By defining the width regarding the quantity of data points, (i.e., in this work we used the 3 by 3 for a single spike in the data points for the tolerance), this filter automatically set the tolerance for the attributes. In the absence of any tolerance value, the algorithm also uses a fraction of the data range as default value most, especially when working with a gridded data such as we have.

By alternating the Derivatives of Euler's Equations inside the Analytical Signal Equations, estimates of the source parameters such as; depths and structural indices could be obtained using the following Equations:
For depths;

$$\frac{(AS1 \times AS2)}{(AS2 \times AS0)\text{-}(AS1 \times AS1)} \mid x = x_0, y = y_0 \qquad 1$$

For SI

$$\frac{(2 \times AS1 \times AS1 \text{ - } AS2 \times AS0)}{(AS2 \times AS0 \text{ - } AS1 \times AS1)} \mid x = x_0, y = y_0 \qquad 2$$

Where;

$$AS0(x, y) = \sqrt{\left(\frac{dT}{dx}\right)^2 + \left(\frac{dT}{dy}\right)^2 + \left(\frac{dT}{dz}\right)^2} \qquad (i)$$

$$AS1(x, y) = \sqrt{\left(\frac{dT}{dxdz}\right)^2 + \left(\frac{dT}{dydz}\right)^2 + \left(\frac{dT}{dzdz}\right)^2} \qquad (ii)$$

$$AS2(x, y) \sqrt{\left(\frac{dT}{dxdzdz}\right)^2 + \left(\frac{dT}{dydzdz}\right)^2 + \left(\frac{dT}{dzdzdz}\right)^2} \qquad (iii)$$

This, therefore, implies that;

$$f(x, y) = \left\{ \begin{matrix} 1 \text{ for } (x, y) \in C_p \\ 0 \text{ or otherwise} \end{matrix} \right\} \qquad 3$$

where C_p is either a closed curl or a closed plane figure.
Equation (4) gives the mathematical representation or the system function of this filter.

$$A(x, y) = [1 - 0.5(\cos(jx) + \cos(iy))] \qquad 4$$

The horizontal gradient of the magnetic data was improved, and International Geomagnetic Reference Field (IGRS) removed. Reduction to the Pole magnetic shaded land features map, Figure3, was applied to the acquired data. It is necessary as the shape of the magnetic anomaly is a function of the original body and the vector orientation. The filtering technique helps to eliminate the effects of interference from other neighbouring magnetic anomaly bodies [22]. This process was carried out with the application of Equation (5);

$$fp(m, n, z) = \frac{1}{4\pi^2} \int\int_{-\infty}^{\infty} Ap(x, y) F_T(x, y, z) e^{j(xp+yq))} dxdy \qquad 5$$

where $A_p(x,y)$ is the filter response for the field reduced to the pole.

Considering the angle of declination, δ; and that of Inclination, *In*, the filter response is given by the expressed in Equation (6) shown below;

$$Ap(x, \theta) = \frac{1}{(j \cos l \sin(\delta + \theta) \text{-} \rho)(j \cos In_0 \sin(\delta_0 + \theta) \text{ - } \rho_0)} \qquad 6$$

where δ_0 and In_0 are respectively the angles of declination and Inclination of the earth's magnetic field vector in the study area.
Conversely, for the purpose of this study, the area lies within the low latitude zone. For this reason, ρ and ρ_0 are respectively approximately zero, by this; the filter response

reduces to Equation (7) as shown below;

$$Ap(x, \theta) = \frac{1}{\sin(\delta + \theta)\sin(\delta_0 + \theta)} \quad 7$$

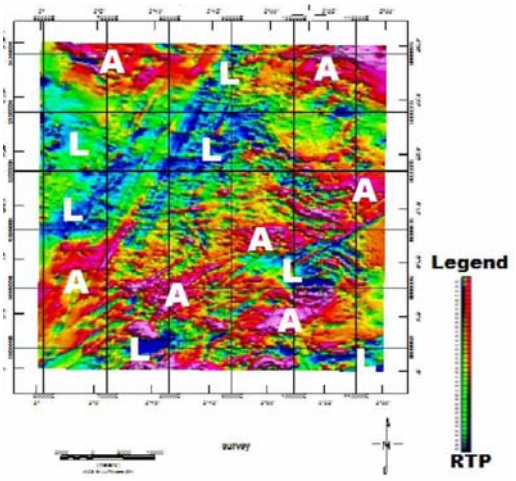

Figure 3. Reduced to the pole (RTP) Total Magnetic Intensity (TMI) Map of the study area as interpreted from Oasis Montaj Software.

Also, the magnetic vertical and horizontal gradients were measured and the Analytical signal map presented in Figure 4. To achieved this, the Oasis Montaj 8.3 software packages that permitted the determination of the angle of dip, the depths to the magnetic anomalies sources, the source edge detection together with the susceptibility contrasts of the causative bodies. To designed a homogeneous function of the N^{th} degree, showed that for N+1 degree of homogeneity, the Euler's Deconvolution Equation becomes the expression as shown in Equation (8);

$$-AN = (x - x_0)\frac{dA}{dx} + (y - y_0)\frac{dA}{dy} + (z - z_0) \quad 8$$

where A = the analytical signal, (AS) of the magnetic anomaly field.

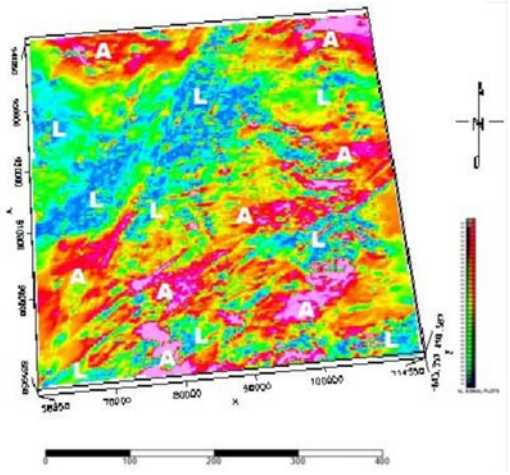

Figure 4. Analytical Signal map generated from Oasis Montaj after the application of the necessary filters.

Thus, to resolve the source parameters; [25], offered in his work, the analytical signal over a magnetic contact as shown in Equation (9) below;

$$A(x, z) = \alpha \frac{1}{\left[(x - x_0)^2 + (z - z_0)^2\right]^{\frac{1}{2}}} \quad 9$$

where x_o and z_o are the respective location and depths of the magnetic contact anomalies. For a two-dimensional (2-D), magnetic sheet anomalies, [25], gave the analytical signal as shown in Equation 10;

$$A(x, z) = \alpha \frac{2}{\left[(x - x_0)^2 + (z - z_0)^2\right]^{\frac{3}{2}}} \quad 10$$

The quantity, α, is resolved using the Equation 11 shown below;

$$\alpha = 2kFc \sin d \quad 11$$

From Equation 11, k = susceptibility of the magnetic anomalies; F = Earth's magnetic fields amid the declination angle,d, and c = constant for horizontal, total and vertical magnetic fields.

Thus, standard structural indices for various earth geological models are as presented in Table 1, [24, 25, 26, 27, 28, 29, 30, 31, 32]. It is expected that various magnetic anomaly sources are capable of having identical structural indices that could be separated without difficulties locally.

Table 1. Structural Indices of amagnetic anomaly for different structural Models.

Magnetic Anomaly	Structural Index (SI)	Unlimited Topological Dimensions
Rock contact	0.5	3 (X, Y, and Z)
Dyke	1.0	2 (Z, and X or Y)
Sill	1.5	2 (X and Y)
Cylinder	2.0	1 (X or Y)
Pipe	2.5	1 (Z)
Sphere	3.0	0

The offset correction between magnetic anomalies and their source rocks, the angles of inclination and declination for Nigerian basement structures varied respectively between 7°N and 13°S and significantly affect the inclination of earth's magnetic fields at a certain point, [26]. The reduced to the pole map was formed on this basis using a geomagnetic inclination and declination angles. The residual field was produced by removing the long wavelengths magnetic anomalies that are referred to as the regional magnetic anomaly from the reduced to the pole data. The lineaments within the area (Figure. 5) were thus delineated from the LANDSAT™8 map. Euler Deconvolution and Tilt angle techniques, [33], were performed on the upward continuation to about 4.1 km of the residual data (Figure 4) to (or "intending to") mapping the basement structures. Furthermore, Structural Index of 0, maximum percentage tolerance of about 15 and window size of 3 by 3 was engaged in the Euler Deconvolution processes.

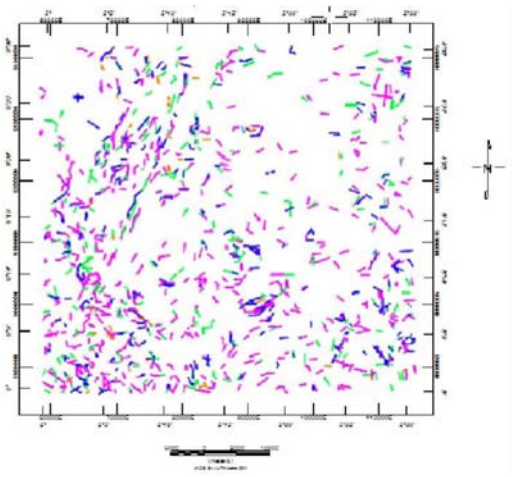

Figure 5. Lineaments map of the study area as delineated from LANDSAT™8data.

3. RESULTS AND DISCUSSION

The subsurface magnetic anomaly structures as delineated in the study area and presented the results of Figures 3 and 4. These maps demonstrate deviations in the magnetic intensity that replicates the magnetic susceptibility of the various subsurface rock units across the diverse terrains present in the Omu-Aran Schist belt. The magnetic intensity map of the study area shows high magnetic values that ranged between about 50-551.205nT, that have power and influence over the north-east, north-west and south-western areas on the map, with light to deep red colors as an indications of reasonably high magnetic susceptibility subsurface rocks being present there which is characteristic of crystalline basement rocks (i.e., hornblende granite and migmatite gneisses). Similarly, low magnetic intensity values that ranged between about 0 to -643.498nT, dominated the west, north-west, and some places in southern

and south-eastern parts on the maps, with green to deep blue colours as a suggestion of subsurface materials of low magnetic susceptibility (i.e., meta-sediments), that overlain the bedrocks.

The minimum total magnetic intensity value of -643.498nT was recorded mostly along the central flank and some pocket places in the north-western and south-eastern flanks. The highest value of 551.205nT recorded mainly in the northern and southern flanks of the study area could be ascribed as the basement complex granitic intrusions. The linear subsurface features obtained from the LANDSAT™ map, (Figure 5), correlates well with the trends obtained in the magnetic maps that would be studied in detail to delineate the features of the geology of the area.

In potential fields (Gravity and Magnetic Methods), the rate at which the source of a given anomaly field geometry drops with the distance is defined as the Structural Index (SI) of the anomaly. There are other methods through which suitable values of structural indices could be decided by selecting some unlimited or great values and agreeable to an extensive measure of spatial degree as shown in a given standard. Therefore, the standard value of the structural index (SI) obtained by these methods is, that standard number minus the upper limits permitted for a particular field, i.e., 3 in the case of a magnetic anomaly data or 2 when considering gravity anomaly data.

Some situations emerged when SI is equal to zero; this insinuates that the magnetic effects are regularly recurrent (i.e., unchanged) irrespective of the position of the anomaly source producing the fields. It is very possible to come close to this limit as the unlimited topological measures of the magnetic anomaly source enlarged. Although, it may be practically unattainable with actual data. Potentially, 0.5 SI are frequently applied to an accomplished plausible conclusion as an alternative to 0SI. In this case, we applied vertical derivative filter first before the other filters during the processing stage.

The results of this study are as presented in Figures 6-11 for the various structural indices. The technique automatically computed the easting and northing coordinates at x and y *directions*, and the depth estimated along the z-directions at every data points and plotted same as 3-D maps. Rock contacts were delineated as SI of 0.5 with three Topological dimensions of x, y, and z at a maximum depth of about 1km, (Figure 6). Dykes were delineated as SI of 1.0 as shown in Figure 7. The maximum depth obtained at this structural index is 1km with two-dimensional topological structures of either a combination of z and x or y. The structural index of 1.5 was ascribed to Sill, which was delineated at a depth of about 1km with two-dimensional topological structures of x and y only, i.e., Figure 8. Horizontal or Vertical Cylindrical structures was delineated at a depth of about 1km with a structural index of 2.0 and a one-dimensional topological shape of either x or y, i.e., Figure 9. Pipe structural shapes were delineated as 2.5 SI along a one-dimensional topological structure of z and a maximum depth of about 1.1km as shown in Figure 10. Spherical subsurface magnetic anomaly structures were delineated as 3.0SI at a maximum depth of about 1.05km and zero-dimensional topological structures as presented in Figure 11.

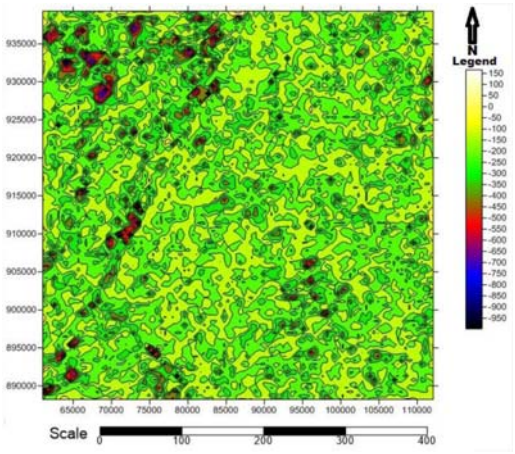

Figure 6. Structural index = 0.5 of the study area at a maximum depth of 1Km.

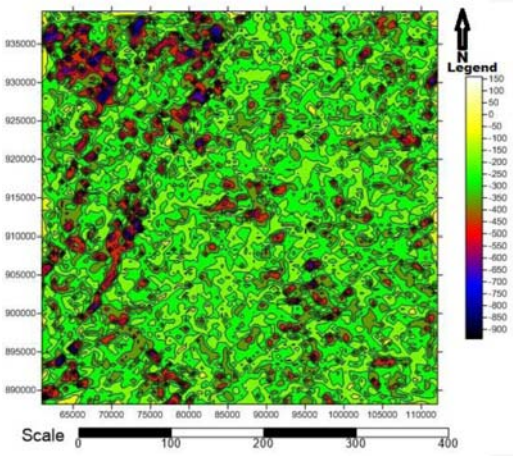

Figure 7. Structural index = 1.0 of the study area at a maximum depth of 1Km.

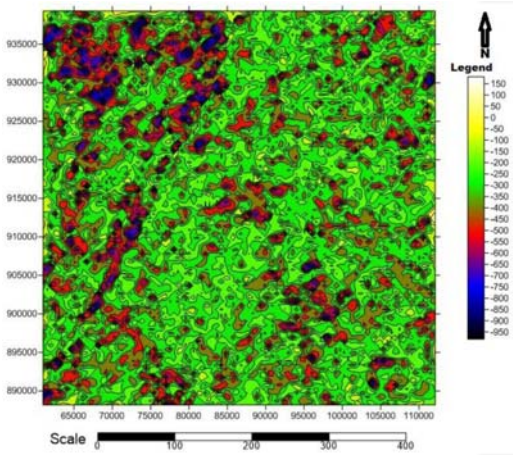

Figure 8. Structural index = 1.5 of the study area at a maximum depth of 1Km.

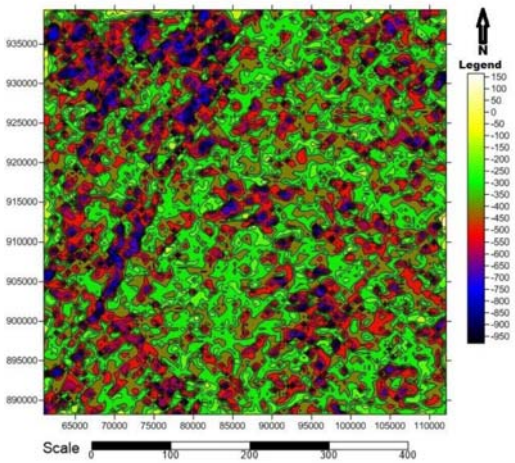

Figure 9. Structural index = 2.0 of the study area at a maximum depth of 1Km.

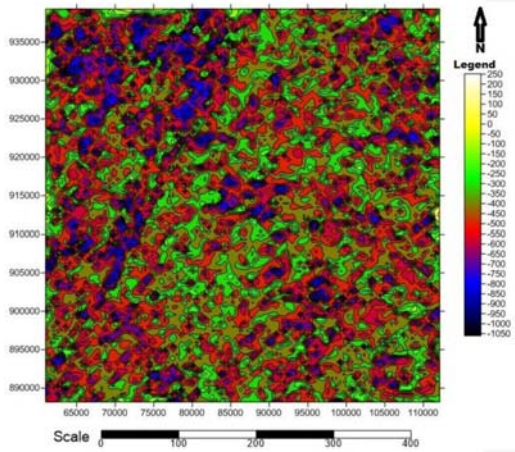

Figure 10. Structural index = 2.5 of the study area at a maximum depth of 1.1Km.

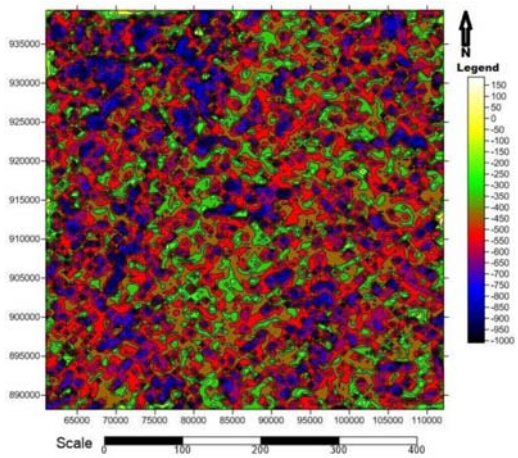

Figure 11. Structural index = 3.0 of the study area at a maximum depth of 1.05Km.

4. CONCLUSION

The report of this study as presented here has tried to correctly apply 3-D Euler Deconvolution technique to outline subsurface magnetic anomalies Ore rock body in the study area. Analysis of the results delineates some magnetised Ore rock bodies accountable for the observed magnetic anomalies in this area. Diverse magnetic basement geological structural features were displayed as maps shown in Figures 3, 4 and 5, through different magnetisations and alignments. The varieties of subsurface geological structural models obtained in the Omu-Aran Schist belt termed "magnetic anomaly basement."

The existence of the Precambrian rocks, (i.e., mafic and ultramafics rocks) as delineated in Omu-Aran area, confer an extraordinary possibility to determine the magnetic anomaly basement structures existing in the area by their nature, spatial alliance, and growth potentially. The technique adopted for this study accordingly enhanced the subsisting insightful knowledge of the subsurface structural geological model in addition to the depths to the three-dimensional geometry of the causal basement geological Ore rock bodies. Through the help of remote sensing PCI Geomatica 2013 software, we have established in what way the aeromagnetic data interpretation demonstrate a robust correlation with the traditional Analytical Signal method from the Geosoft Oasis Montaj software. This study, therefore, created well-built, solid models of the subsurface geological, magnetic anomalies basement structures in Omu-Aran schist belt zone. The Structural Index Maps, i.e., Figures 6-11, generated are useful devices towards supporting an improved solid mineral exploration in the area through the delineation of various depths to the subsurface structures that hosted these minerals.

Suggestions for the outcrop arrangement in the area are short off from the model obtained through the Remote Sensing analysis of the aeromagnetic data in Omu-Aran area. The results signify to a large extent, further broad structural features of the subsurface environment. The most important parameters that are targeted for the emplacement and promoting subsurface geological, magnetic anomalies basement structural rock units are faulted plains; fractured bedrocks, contacts between two or more subsurface rock bodies, and intrusions during tectonic activities. This study clearly delineated these complex basement features in the area as shown in Figures 3-5 and marked as A, (i.e., high magnetic intensity values zones) and L, (i.e., Low magnetic intensity zones).

Figures 6-11, make available an idea of modelled depths in addition to the structural index map within which the entire locality linked through magnetic anomaly Ore rock units were allotted the same value of depths, or else, the structural indices. The knowledge of the characteristics of the subsurface basement sources of the magnetic Ore rock bodies in Omu-Aran area is then achieved using the source edge location parameters of the depths and structural indices. Better results were obtained through these techniques compares to the conventional methods of depths determinations, e.g., Slope methods. This is because automatic depths determination is more accurate with minimal errors than the conventional computations from slopes methods of the edges determinations, i.e. Peter's half-slope or straight slope methods.

ACKNOWLEDGMENTS

The authors are grateful to the Universiti Sains Malaysia, School of Physics, Geophysics Unit, and the IPS for the Postgraduate Fellowship supports towards the doctoral research program.

REFERENCES

[1] Kearey P., Brooks M. and Hill I., *An Introduction to Geophysical Exploration*, John Wiley & Sons, New York, 2013.

[2] Osinowo O.O., Akanji A.O. and Olayinka A.I.*J., Afr. Earth Sci*., 2014; DOI 10.1016/j.jafrearsci.2013.11.005.

[3] Abedi M., Gholami A. and Norouzi G.H., *Comp. Geosci.,* 2013; **52**: 269-280. DOI 10.1016/j.cageo.2012.11.006.

[4] MMSD. *In:* Agency, N.G.S. (ed.). Abuja, Nigeria, 2010.

[5] Ako B., *J. Min. Geol.,* 1980; **17**: 129-138.

[6] Ajayi T., *Nigeria J. Min. Geol.,* 1980; **17**: 179-196.

[7] Annor A.E., Olobaniyi S.B. and Mucke A., *J. Afr. Earth Sci.,* 1997; **24**: 39-50. DOI 10.1016/S0899-5362(97)00025-0.

[8] Obaje N.G., *Geology and Mineral Resources of Nigeria,* Springer-Verlag Berlin Heidelberg, 2009. DOI 10.1007/978-3-540-92685-66,

[9] Rahaman M., *Prec. Geol. Nigeria*, 1988; 11-41.

[10] Caby R. and Boesse J., *J. Afr. Earth Sci.,* 2001; **33**: 211-225. DOI 10.1016/S0899-5362(01)80060-9.

[11] Woakes M., Rahaman M. and Ajibade A., *J. Afr. Earth Sci.,*1983; **6**: 655-664. DOI 10.1016/0899-5362(87)90004-2.

[12] Oyinloye A.O., *J. Afr. Earth Sci.,* 1998; **26**: 633-641. DOI 10.1016/S0899-5362(98)00037-2.

[13] Olasehinde P., Pal P. andAnnor A., *J. Afr. Earth Sci.,* 1990; **11**: 351-355. DOI 10.1016/0899-5362(90) 90014-6.

[14] Olade M. and Elueze A., *Prec. Res.,* 1979; **8**: 303-318. DOI 10.1016/0301-9268 (79)90033-0.

[15] Scheidegger A.E. and Ajakaiye D.E., *J. Afr. Earth Sci,*. 1985; **3**: 461-470. DOI 10.1016/S0899-5362(85)80089-0.

[16] Adepelumi A., Ako B., Ajayi T., Olorunfemi A., Awoyemi M. and Falebita D., *J. Afr. Earth Sci.,* 2008; **52**: 161-166. DOI 10.1016/j.jafrearsci.2008.07.002.

[17] Ten Brink U.S., Rybakov M., Alzoubi A.S. and Rotstein Y., *Geochem. Geophy. Geosys.,* 2007; **8**. DOI 10.1029/2007GC001582.

[18] Megwara J.U. and Udensi E.E., *Earth Sci. Res.,* 2014; **3**: 27.

[19] Ayodele O. and Odeyemi I., *Ind. J. Sci. Technol.,* 2010; **3**: 31-36. DOI 10.17485/ijst/2010/v3i1/29639.

[20] Naidu P. and Mathew M., *Analysis of Geophysical Potential Fields. A Digital Signal Processing Approach,* Elsevier, Amsterdam, 1998.

[21] Fraser D., Fuller B. and Ward S., *Geophysics,* 1966; **31**: 1066-1077. DOI 10.1190/1.1439840.

[22] Geosoft, *Geosoft Inc. ver. 8.3*. Toronto, Ontario, 2014.

[23] Naudy H. and Dreyer H., *Geol. Pros.,* 1968; **16**: 171-178. DOI 10.1190/1.1439840.

[24] Reeves C., *Aeromagnetic Surveys: Principles, Practice and Interpretation*, Geosoft. Toronto, Ontario, 2005.

[25] Thompson D.T., *Geophysics,* 1982; **47**: 31-37. DOI 10.1190/1.1441278.

[26] Macleod I., Jones K. and Dai T., *Expl. Geop.,* 1993; **24**: 679-688. DOI 10.1071/EG993679.

[27] Durrheim R. and Cooper G., *Comp. Geosci.,* 1998; **24**: 545-550. DOI 10.1016/S0098-3004(98)00022-3.

[28] Barbosa V.C., Silva J.B. and Medeiros W.E., *Geophysics,* 1999; **64**: 48-60. DOI 10.1190/1.1444529.

[29] Bayrak M., *J. Balkan Geop. Soc.,* 2002; **5**: 35-46.

[30] Cooper G., *Expl. Geop.,* 2004; **35:** 165-170. DOI 10.1071/EG04165.

[31] Doo W.B., Hsu S.K. and Yeh Y.C., *Geop. Pros.,* 2007; **55**: 255-264. DOI 10.1111/j.1365-2478.2007.00603.x.

[32] Davis K., LI Y. and Nabighian M., *Geophysics,* 2010; **75**: G13-G20. DOI 10.1190/1.3375235.

[33] Salem A., Williams S., Fairhead D., Smith R. and Ravat D., *Geophysics,* 2007; **73**: L1-L10. DOI 10.1190/1.2799992.